Bio-Design and Manufacturing (2025) 8:391–409
https://doi.org/10.1631/bdm.2400176

RESEARCH ARTICLE

Polypeptide-modified black phosphorus nanosheets as a brain-targeted neuroprotective agent for treating ischemic stroke

Meili Zhang[1] · Taojian Fan[2] · Shujiang Yin[1] · Jie Li[1] · Jing Hou[1] · Ke Zhang[1] · Bo Han[1] · Wen Chen[1] · Han Zhang[2] · Xing Tian[1]

Received: 5 May 2024 / Accepted: 21 September 2024

Abstract

Ischemic stroke is the leading cause of death in China, accounting for approximately one-third of all stroke-associated deaths worldwide. Currently, thrombolysis is employed for ischemic strokes. However, due to the limited therapeutic window of thrombolytic agents, most patients do not receive the drug at the right time. Moreover, these agents are associated with risks of hemorrhage and reperfusion damage. Herein, Angiopep-2 (ANG)-black phosphorus (BP)-resveratrol (RES), a drug-loaded system, was used to deliver drugs across the blood–brain barrier (BBB). ANG-BP-RES has a uniform size, stable structure, good photothermal effect, and strong drug release ability under near-infrared (NIR) irradiation and acidic conditions. Furthermore, ANG-BP-RES can efficiently target the brain and improve BBB permeability, exerting a significant therapeutic effect against ischemic brain injury, especially after NIR irradiation. ANG-BP-RES is also biocompatible and shows minimal toxicity toward cells and tissues. This study offers novel insights into the therapeutic management of ischemic brain injury.

✉ Han Zhang
hzhang@szu.edu.cn

✉ Xing Tian
tianxingdeyoujian@163.com

[1] Key Laboratory of Xinjiang Phytomedicine Resource and Utilization of Ministry of Education, School of Pharmacy, Shihezi University, Shihezi 832002, China

[2] College of Physics and Optoelectronic Engineering, Shenzhen University, Shenzhen 518000, China

Graphical abstract

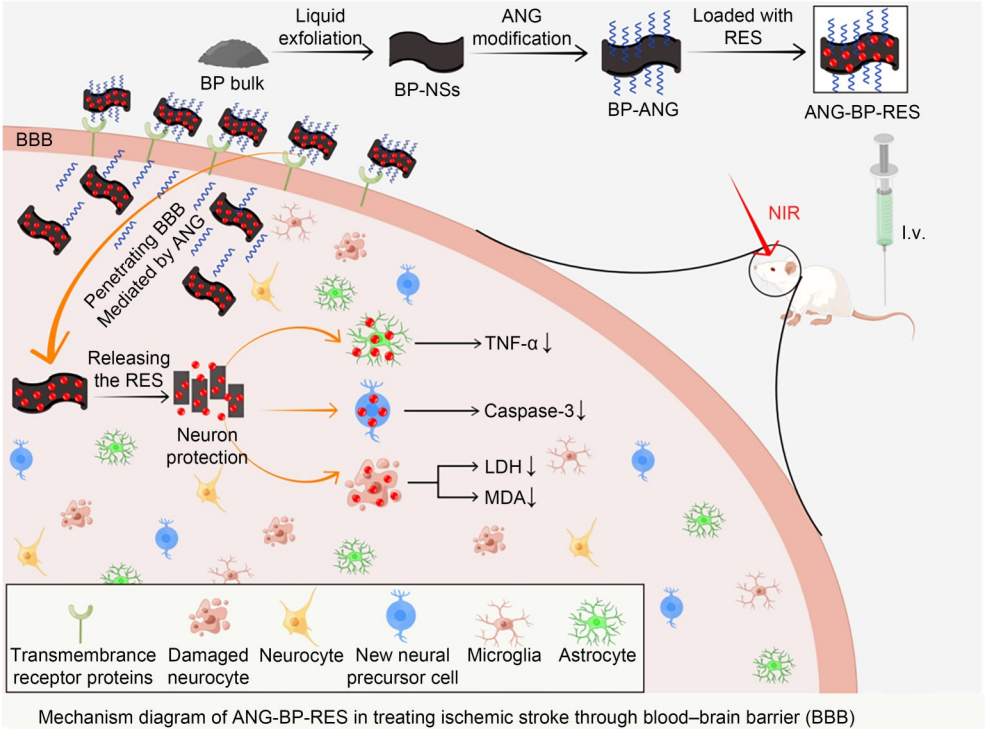

Mechanism diagram of ANG-BP-RES in treating ischemic stroke through blood–brain barrier (BBB)

Keywords Black phosphorus nanosheets · Resveratrol · Polypeptide · Ischemic stroke · Blood–brain barrier · Drug delivery system

1 Introduction

Cerebrovascular diseases pose a global health challenge with high mortality and disability rates [1]. These diseases are divided into ischemic and hemorrhagic events, with ischemic diseases accounting for over 60% of all cerebrovascular diseases [2]. Ischemic brain injury is characterized by insufficient blood supply to the brain, leading to cerebral ischemia. Narrowing or occlusion of the carotid, vertebral, and other cerebral arteries affects the blood supply to the brain, leading to ischemia, hypoxia, and necrosis of the brain tissues [3, 4]. Cerebrovascular diseases remain challenging to treat because most drugs cannot effectively cross the blood–brain barrier (BBB) [5]. The recombinant human tissue plasminogen activator (tPA) is the only drug approved by the Food and Drug Administration to manage ischemic stroke [6]. However, this drug has a narrow therapeutic window, and only 7% of patients meet the therapeutic criteria [4]. Although the latest research has increased the time window of endovascular treatment to 24 h [7, 8], many medical centers cannot meet the requirements for medical equipment and personnel allocation, which limits the beneficiaries. Therefore, prompt use of neuroprotective therapy alone or in combination to reduce nerve injury will effectively improve the prognosis of patients and reduce the burden on society and families. Therefore, novel therapeutic options and drug delivery systems need to be urgently developed [9].

Researchers have established various approaches to enhance the transport across the BBB, thereby improving the therapeutic efficacy of drugs in cerebrovascular diseases. An ideal delivery system should have minimal side effects and achieve adequate drug concentrations in the brain [10, 11]. A nanodelivery system is a promising approach for enhancing drug permeability across the BBB [12–14]. Recent studies have shown that black phosphorus (BP) nanosheets have great potential for photothermal therapy, photoacoustic imaging, and fluorescence imaging because of their strong interaction with light [15–17]. The extinction coefficients, photothermal conversion efficiency, and fluorescence quantum yield in the near-infrared (NIR) region of these BP nanosheets are high [18, 19]. Sun et al. revealed that BP quantum dots (BPQDs), with an average size of (2.6±1.8) nm, were rapidly eliminated by the kidneys,

thereby preventing long-term toxicity [20]. Moreover, cell experiments showed that the subminiature BPQDs had an effective photothermal killing effect and good biocompatibility. Furthermore, Tao et al. [18] showed that BP had a drug loading capacity of 108%, which was much higher than that of traditional nanomaterials. BP nanosheets can achieve precise loading and controlled drug release through response to light stimuli [21]. BP can also be degraded into phosphate, a ubiquitous metabolite in the body [22]. Therefore, BP is a promising material for developing drug delivery systems.

This study investigated the therapeutic effects of resveratrol (RES) delivered using a BP nano-tablet delivery system [23] in ischemic stroke. Research interest in developing RES has recently increased due to its extensive biological activities. RES exerts its therapeutic effects through its antioxidant [24], anti-inflammatory [25], cardioprotective [26], and anticancer [27] properties. These effects of RES have been investigated in various diseases, including obesity, diabetes, cardiovascular diseases [28], and more recently, nerve protection and regeneration [29]. For example, RES was shown to mediate nerve regeneration and motor repair in a rat model of sciatic nerve crush injury [30], proving its ability to ameliorate spinal cord injury [31]. However, the clinical applications of RES are limited due to its low solubility [32], poor stability after exposure to light, oxygen, high temperatures, and oxidase enzymes [33], rapid degradation in the body [34], low activity levels under various environmental and physiological conditions [35], and inability to be metabolized or absorbed by the body [36].

Angiopep-2 (ANG; TFFYGGSRGKRNNFKTEEY), a novel polypeptide comprising 19 amino acids, acts as a ligand for low-density lipoprotein receptor-related protein 1 (LRP-1) on the blood-cerebrospinal fluid barrier (BCSFB) [37]. ANG is derived from the peptide inhibitory protein and other Kunitz domains of human proteins [38] that can penetrate the brain via endocytosis mediated by LRP-1. ANG also shows brain-targeting characteristics [38]. Previous studies have shown that carriers, such as liposomes [39] and polymer nanoparticles modified by ANG [40], increase drug permeability across the BBB. Further, Phases 1 and 2 in clinical trials revealed a higher brain intake of drugs delivered along with ANG [41, 42]. In summary, ANG can be used to improve the brain-targeting ability of drugs.

In this study, uniformly-sized low-level BP was prepared using a liquid phase stripping method. Subsequently, the BP was modified using ANG to improve its brain-targeting ability and loaded with RES to construct a brain-targeting BP drug delivery system (Fig. 1). This study aimed to investigate the neuroprotective effects of RES against oxidative damage induced by ischemia–reperfusion in mice.

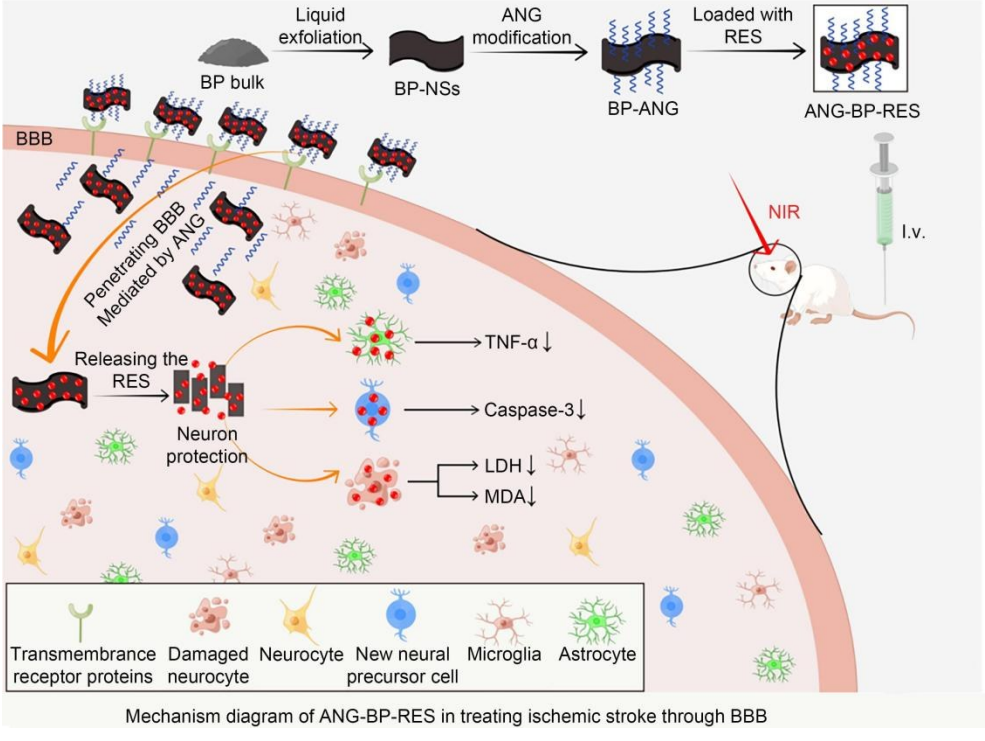

Fig. 1 Schematics of the structure of the peptide-modified brain-targeted BP nano-tablet delivery system (ANG-BP-RES) and its mechanism of anti-ischemic brain injury. Polypeptide-modified BP nanosheets can release drug RES in brain tissue through the blood–brain barrier (BBB) under the action of ANG, which can inhibit the expression of caspase-3 and TNF-α in brain tissue and the release of LDH and MDA in brain cells, thus playing a neuroprotective role and producing an anti-ischemic brain injury effect. TNF-α: tumor necrosis factor-α; LDH: lactate dehydrogenase; MDA: malondialdehyde; NS: nano-sheet

2 Materials and methods

2.1 Materials

BP powder and N-methyl pyrrolidone (NMP) were purchased from Nanjing Xianfeng Nanomaterials Technology Co. (China) and Shanghai Maclean Biochemical Technology Co. (China), respectively. RES and heparin sodium were procured from Anhui Zesheng Technology Co. (China). ANG (TFFYGGSRGKRNNFKTEEY) and the fluorescent protein Cy5.5 (Cy5.5-PEG-NH_2) were obtained from Guangzhou Carbon Water Technology Co. (China). Sodium bicarbonate ($NaHCO_3$) and disodium edetate (EDTA-2Na) were from Tianjin Sheng'ao Chemical Reagent Co. (China). Anhydrous ethanol was from Tianjin Windship Chemical Reagent Technology Co. (China). Physiological saline was purchased from Sichuan Keren Pharmaceutical Co. (China). Phosphate-buffered saline (PBS) and the hematoxylin-eosin (H&E) staining kit were purchased from Beijing Solaibao Technology Co. (China). Surgical instruments and thread plugs were from Beijing Surgno Technology Co. (China).

2.2 Synthesis of BP nanosheets

BP nanosheets were prepared using the liquid phase stripping method. Briefly, 0.1 g of BP powder was thoroughly ground in a mortar and washed using an ultrasonic cleaner (power: 500 W) for 12 h. During the process, water was continuously changed to ensure a low-temperature state. The ultrasonication was continued in a cell disruptor at a power of 500 W for 1 h. The upper layer of the static suspension was centrifuged at 2000 r/min and 4 °C for 5 min. Furthermore, the upper liquid layer was centrifuged twice at 15 000 r/min and 4 °C. Finally, the NMP was removed and replaced with a similar volume of PBS to obtain the BP suspension.

2.3 Synthesis of BP-ANG

To synthesize BP-ANG, 10 mg of ANG-PEG-NH_2 was added to 5 mL of BP/PBS solution (200 μg/mL BP), continuously stirred for 8 h, and centrifuged at 10 000 r/min for 15 min at 4 °C to remove excess ANG-PEG-NH_2. After that, the sample was washed twice with PBS, as previously described. The residue was redissolved in PBS and stored at 4 °C.

2.4 Synthesis of ANG-BP-RES

The BP-ANG solution was constantly mixed with 5 mL of RES (2 mg/mL ethanol) at room temperature for 24 h. Then, the mixture was centrifuged at 10 000 r/min for 15 min at 4 °C to remove any free RES. After discarding the supernatant, the residue was washed twice with PBS. The precipitated ANG-BP-RES was resuspended in PBS and stored at 4 °C.

2.5 Synthesis of BP-Cy5.5 and ANG-BP-Cy5.5

Cy5.5-PEG-NH_2 was used to label BP and BP-ANG for in vitro and in vivo fluorescence imaging. BP-Cy5.5 and ANG-BP-Cy5.5 were synthesized by mixing 10 mg of Cy5.5-PEG-NH_2 with 5 mL of BP or BP-ANG (200 μg/mL) formulations, respectively. After stirring the mixture for 8 h, it was centrifuged to remove free Cy5.5-PEG-NH_2 and then washed twice with PBS.

2.6 Characterization of BP preparations

The peptide-modified brain-targeted drug delivery system, ANG-BP-RES, was characterized using a Malvin particle size analyzer, transmission electron microscopy (TEM), scanning electron microscopy (SEM), ultraviolet and visible spectrum (UV-Vis), and Fourier transform infrared spectroscopy (FTIR) to verify whether the BP nanoparticles were successfully modified and loaded with RES.

2.7 In vitro drug release study

The ANG-BP-RES solution was placed into dialysis bags (molecular weight cut off: 14 kDa) and immersed in 100 mL PBS solutions with different pH values (pH: 5.0, 5.8, and 7.4). To determine the amount of RES released by ANG-BP-RES, 1 mL of dialysate was collected at different time points (the dialysis bags were rehydrated after collecting the dialysate). NIR irradiation was performed under the same pH conditions (pH: 5.0, 5.8, and 7.4) to study the NIR-triggered release of RES. Before the dialysis, the solution was irradiated with an 808-nm NIR laser with a power density of 1 W/cm^2 for 10 min. Then, 1 mL of dialysate outside the dialysis bag was collected at an appropriate time point to measure the absorbance at 306 nm.

2.8 Measurement of photothermal performance

Various concentrations (25, 50, 100, and 200 μg/mL) of PBS, BP, BP-ANG, and ANG-BP-RES solutions were irradiated with NIR (808 nm, 1 W/cm^2) for 8 min. The temperature was recorded every 10 s, and the temperature changes for each group within the first 8 min were compared. Similarly, these preparations were irradiated with NIR at different power densities (0.2, 0.5, 1.0, and 2.0 W/cm^2) for 10 min, and the temperature was recorded

every 10 s. The temperature changes in each group were compared.

To further assess the photothermal performance of an equivalent quantity of ANG-BP-RES, the BP, BP-ANG, and ANG-BP-RES solutions were irradiated with an 808-nm NIR laser with a power density of 1.0 W/cm^2 for five cycles. During each cycle, the solution was irradiated for 10 min and allowed to cool for 10 min. The maximum temperature obtained during each cycle was compared while the temperature variations of the BP, BP-ANG, and ANG-BP-RES solutions were monitored.

2.9 Evaluation of in vitro cytotoxicity

Human neuroblastoma (SH-SY5Y) cells were inoculated into 96-well plates and cultured for 24 h at 37 °C and 5% CO_2 to investigate the cytotoxicity of RES, BP, and ANG-BP-RES. After discarding the old culture medium, 200 μL of fresh medium was added at different concentrations (0–200 μg/mL), and the cells were cultured for 24 h. Further, a blank group and an NIR irradiation group were established. Cells in the blank control group were co-cultured with PBS solution, while those in the NIR group were irradiated with the NIR laser (808 nm, 1 W/cm^2) for 5 min before co-culturing with different concentrations of RES, BP, ANG-BP-RES, and ANG-BP-RES+NIR (1, 5, 10, 20, 50, 100, 150, and 200 μg/mL).

Following the co-culture, the old medium was replaced with 200 μL of fresh medium containing 10% fetal bovine serum. After that, 20 μL of cell counting kit-8 (CCK-8) solution was added to each well, and the solution was vacuumed into 96-well plates and cultured in an incubator for 2 h. Subsequently, the enzyme label was added, and the absorbance was recorded at 450 nm. The blank control group comprised CCK-8 and culture media without the cells. The cell viability was calculated using Eq. (1):

$$\text{Cell viability} = \frac{A_{\text{sample}} - A_{\text{blank}}}{A_{\text{control}} - A_{\text{blank}}} \times 100\%, \quad (1)$$

where A_{sample}, A_{blank}, and A_{control} are the absorbance values of the sample, the blank group, and the control group, respectively.

2.10 In vitro assessment of neuroprotection

2.10.1 Determining the appropriate glutamic acid concentration for modeling

In the model group, SH-SY5Y cells were first cultured with 100 μL complete medium for 6 h, and then for 18 h with different concentrations of glutamic acid (1.25, 2.5, 5, 10, 20, and 30 mmol/L). After removing the culture medium, each well was washed with PBS three times. Then, 100 μL culture medium containing 10% CCK-8 was added to each well, and the plates were cultured in a 5% CO_2-containing incubator at 37 °C for 2 h. Subsequently, 75 μL of solution was drawn from each well and transferred into a 96-well plate. The cell activity at different glutamic acid concentrations was determined using an enzyme-labeled instrument. The appropriate glutamic acid concentration was selected for modeling.

2.10.2 Detection of activity changes in nerve cells

In the model group, SH-SY5Y cells were cultured with different concentrations (1, 5, 10, 20, 50, and 100 μg/mL) of RES, BP-RES, BP-RES+NIR, ANG-BP-RES, and ANG-BP-RES+NIR, and appropriate concentrations of glutamic acid for 18 h. Cell viability was determined using the CCK-8 assay. The cells in the ANG-BP-RES+NIR group were stained for alive/dead assay and observed using a laser scanning confocal microscope.

2.10.3 Detection of lactate dehydrogenase (LDH) and malondialdehyde (MDA) release from nerve cells

SH-SY5Y cells were co-cultured with drug solvent for 6 h and then with 20 mmol/L glutamic acid for 18 h (model group). SH-SY5Y cells were co-cultured with different concentrations (1, 5, 10, 20, 50, and 100 μg/mL of RES, BP-RES, BP-RES+NIR, ANG-BP-RES, and ANG-BP-RES+NIR) (administration group). After the co-culture, the release of LDH and MDA from both groups was detected using LDH enzyme-linked immunosorbent assay (ELISA) detection kit and mouse MDA ELISA kit. The results obtained in RES, BP-RES+NIR, ANG-BP-RES, and ANG-BP-RES+NIR groups were compared in the control group and model group, respectively, to evaluate the protective effect of ANG-BP-RES drug delivery system on nerve cells.

2.11 In vitro assessment of BBB permeability

Briefly, bEnd.3 cells were added to the upper chamber (1× 10^5 per well) of a Transwell plate to form a monolayer. The in vitro BBB permeability was assessed using Cy5.5, BP-Cy5.5, BP-Cy5.5+NIR irradiation, ANG-BP-Cy5.5, and ANG-BP-Cy5.5+NIR irradiation. The culture medium was replaced every other day, and the transepithelial electrical resistance (TEER) was checked until it reached 200 Ω·cm^2. The upper chamber was filled with 500 mL of Dulbecco's modified Eagle medium (DMEM) containing specific preparations (equivalent to the Cy5.5 concentration) and incubated for 4 h. After that, the cell monolayers were irradiated with an NIR laser (808 nm, 1 W/cm^2, 5 min). The Cy5.5 content in the top chamber was measured by UV-Vis absorbance at 678 nm, and a standard curve was plotted.

The level of translocation in the BBB model was determined using Eq. (2):

$$\text{Permeability} = \frac{C_b - C_a}{C_b} \times 100\%, \quad (2)$$

where C_b and C_a indicate the concentrations of Cy5.5 in the upper chamber before and after incubation, respectively.

2.12 Animals

Six- to eight-week-old specific pathogen-free male Kunming mice (weighing (25±5) g) were obtained from the Animal Center of Xinjiang Medical University. The animals were housed under appropriate conditions for adaptation with free access to food and water.

2.12.1 Hemolysis experiment

Red blood cell suspension (100 mL) was obtained from the mice in an Eppendorf tube. The hemolysis experiment was divided into the following five groups: positive control (water), negative control (PBS), RES, BP, and ANG-BP-RES groups. The concentration of RES, BP, and ANG-BP-RES groups ranged between 0 and 200 μg/mL. The cell suspension was incubated at 37 °C for 3 h. Then, 800 μL of PBS was added to each group, shaken thoroughly, and the supernatant was collected. The absorbance was measured at 540 nm using an enzyme-labeled instrument. The hemolysis percentage was calculated using Eq. (3):

$$\text{Hemolysis} = \frac{A_{es} - A_{nc}}{A_{pc} - A_{nc}} \times 100\%, \quad (3)$$

where A_{es} is the absorbance value of the experimental solution, A_{nc} is the absorbance value of the negative control, and A_{pc} is the absorbance value of the positive control.

2.12.2 In vivo fluorescence imaging and biodistribution study

The animals were randomly divided into five groups (n=3): (1) Cy5.5+NIR; (2) BP-Cy5.5; (3) BP-Cy5.5+NIR; (4) ANG-BP-Cy5.5; (5) ANG-BP-Cy5.5+NIR. The animals were treated with Cy5.5 (1 mg/kg) and BP (6 mg/kg). After 30 min, all animals except those in Groups (2) and (4) were irradiated with NIR (808 nm, 1 W/cm^2, 5 min) and subjected to fluorescence imaging at 1, 2, 3, 4, 6, 8, and 24 h following treatment. The primary organs (brain, heart, liver, spleen, lungs, and kidneys) were harvested and fluoroscopically examined every 6 h. The fluorescence intensity of Cy5.5 (a.u.) was measured using ImageJ to show the accumulation of nanosheets in these organs, which was then multiplied by the weight (unit: g) of each organ.

2.12.3 Pharmacokinetic studies

2.12.3.1 Ultra performance liquid chromatography (UPLC) detection of resveratrol

A standard solution of RES was scanned over a wavelength range of 200–800 nm using an ultraviolet spectrophotometer to determine the maximum absorbance wavelength. The chromatographic conditions for the mobile phase were set as follows: acetonitrile:water=35:65; column temperature, 30 °C; sample volume, 1 μL; flow rate, 0.3 μL/min; detection wavelength, 306 nm; column, SunFire C_{18} (5 μm, 150 mm×46 mm).

2.12.3.2 Standard curve of resveratrol

To evaluate the bioavailability of ANG-BP-RES, UPLC was used to measure the drug concentration in the blood and tissues at different time points after administration, and its related pharmacokinetic parameters were calculated. The stock solution of RES was prepared at 1 mg/mL concentration by accurately weighing 10 mg of RES and dissolving it in ethanol in a 10-mL volumetric flask. Furthermore, serial dilutions were made. The drug concentration gradient in plasma was 0.064, 0.320, 0.960, 1.280, 1.600, 3.200, and 9.600 μg/mL, and that in tissues was 0.023, 0.092, 0.184, 0.368, 0.738, 1.480, and 2.958 μg/mL. To preserve stability, the RES solution was prepared in the dark at room temperature. The peak area (the ordinate A as shown in Figs. S9 and S10 in the supplementary information) of RES at various concentrations was calculated and compared with the corresponding drug concentrations in various tissues (Figs. S9 and S10 in the supplementary information) to determine the equation for the standard curve.

2.12.3.3 Determination of blood and tissue drug concentrations

The mice were divided into two groups: ANG-BP-RES+NIR irradiation and RES groups. The mice in the ANG-BP-RES+NIR group received a tail vein injection of ANG-BP-RES at a dose of 30 mg/kg, followed by irradiation with an 808-nm NIR laser (1 W/cm^2, 10 min). The RES group received a tail vein injection of RES (dissolved in normal saline). Plasma samples (n=6) were obtained at 0.083, 0.25, 0.5, 1, 2, 4, 6, 8, and 12 h following the respective treatments. Further, tissue samples (n=3) were collected from the brain, heart, liver, spleen, lungs, and kidneys at 0.25, 0.5, 1, 2, 4, 6, 8, 12, and 24 h after drug treatment. Then, the RES concentration in all samples was determined using UPLC. The pharmacokinetic parameters, including (i) the peak or maximum drug concentration of RES in plasma and brain tissues (C_{max}), (ii) elimination half-life ($T_{1/2}$), which represents the time required for the drug concentration to

decrease by half of the initial concentration after administration, (iii) area under the concentration–time curve of RES in plasma or brain tissue (AUC_{0-t}), and (iv) mean residence time (MRT_{0-t}), were calculated using the DAS (Drug and Statistics) 3.0 software.

2.12.4 In vivo analysis of the anti-ischemic stroke effect of ANG-BP-RES

2.12.4.1 Behavioral evaluation

Mouse models of transient middle cerebral artery occlusion (MCAO) were established and divided into five groups (n=6): the control (sham operation), model (MCAO modeling), RES+NIR, ANG-BP-RES, and ANG-BP-RES+NIR (consisting of mice administered with RES+NIR, ANG-BP-RES, and ANG-BP-RES+NIR, respectively, after MCAO modeling) groups. The behavioral performance of mice was observed at 24 h after the operation and assessed according to Longa's [43] scoring standards. The scores were assigned as follows: 0—mice with no neurobehavioral characteristics; 1—mice who could not fully extend their left forelimb in a prone position; 2—those with left limb paralysis who were prone to falling to the left while walking or experienced rear-end collision; 3—mice who were likely to fall to the left while walking or could not stand alone and occasionally roll to one side; 4—mice without any obstacles on consciousness and behavior of voluntary activities.

2.12.4.2 Measurement of brain water content

The mice were divided into five groups (n=6): the control, model, RES+NIR, ANG-BP-RES, and ANG-BP-RES+NIR groups. The mice were decapitated 24 h after the MCAO modeling and administration. Their brains were removed and weighed before and after oven drying at 60 °C for 24 h to obtain the wet and dry weights. The brain water content in each group was calculated using Eq. (4):

$$\text{Brain water content} = \frac{C_w - C_d}{C_w} \times 100\%, \quad (4)$$

where C_w and C_d denote the weights (unit: mg) of the brain tissue before and after oven drying, respectively.

2.12.4.3 2,3,5-Triphenyltetrazolium chloride (TTC) staining

The mice were divided into five groups (n=3), control, model, RES+NIR, ANG-BP-RES, and ANG-BP-RES+NIR groups. Twenty-four hours after MCAO modeling and administration, the hearts of mice were perfused with normal saline, and the brain tissues were harvested and dissected. The brain and heart tissues were washed and stored in a freezer at −80 °C for 30 min. After that, the brain tissues were evenly cut into five pieces using a cryostat. Subsequently, the brain slices were soaked in 2% TTC solution and incubated in the dark at 37 °C for 30 min, with turning every 5 min. After incubation, the tissues were washed using ultra-pure water and fixed with paraformaldehyde for 12 h. Photographs of the tissues were visualized using the ImageJ software.

2.12.4.4 Immunohistochemical analysis

Mice were divided into five groups (n=3): the control, model, RES+NIR, ANG-BP-RES, and ANG-BP-RES+NIR groups. Twenty-four hours after administration of RES+NIR, ANG-BP-RES, and ANG-BP-RES+NIR, the hearts of mice were perfused with normal saline, and their brain tissues were harvested and dissected. The brain tissues were washed, fixed in 4% paraformaldehyde for 24 h, dehydrated, embedded in liquid paraffin, and then sliced. The brain tissue slices were dyed, dehydrated, air-dried, and then observed under a microscope. The images were analyzed using ImageJ. Furthermore, the cumulative optical density was calculated. The changes in the levels of caspase-3 and tumor necrosis factor-α (TNF-α) in each group were compared to evaluate the effect of the BP nanosheets in reducing ischemic brain injury.

2.13 H&E staining

Male mice were randomly allocated into four groups (n=6): the control, RES, ANG-BP-RES, and ANG-BP-RES+NIR groups. All groups except the control group received daily tail vein injections of 30 mg/kg RES and ANG-BP-RES at regular intervals. The control group received a tail vein injection of the same volume of PBS. The mice were weighed daily before drug administration, and the changes in weight were compared among the groups. The rats were euthanized after continuous administration of the drugs for one week. Then, the hearts of mice were perfused with normal saline. The tissues from the organs were anatomically separated, fixed, embedded in paraffin, cut into slices, dewaxed, stained with H&E, and examined under an optical microscope.

2.14 Statistical analysis

Statistical analysis was performed using SPSS 24.0 software. The data were reported as mean+standard deviation. The independent samples t-test was used for comparison between the two groups. A p-value of <0.05 was considered statistically significant.

3 Results and discussion

3.1 Characterization of BP nanosheet preparation

In this study, a drug delivery system consisting of BP nanotablets modified by a polypeptide ANG and loaded with the therapeutic drug RES was synthesized. This system was characterized using several experiments to confirm its successful preparation. First, the particle size and potential changes of the prepared samples were measured using a Malvin particle size analyzer. The results revealed that the sizes of the BP, polypeptide-modified BP-ANG, and drug-loaded ANG-BP-RES nanosheets were (125.2±9.2), (200.6±8.5), and (238.4±5.8) nm, respectively (Fig. 2a). The zeta potential of the BP, BP-ANG, and ANG-BP-RES nanosheets was (−13.83±0.96), (−17.80±0.54), and (−21.23±0.37) mV, respectively (Fig. 2b). In contrast with pure BP nanosheets, the particle size measured by Malvin particle size analyzer was higher due to the stacking polymerization of ANG-BP-RES after drug loading, as did the electrostatic repulsion between the particles. Subsequently, SEM and TEM analysis of the BP nanosheets revealed a layered structure with an average size of approximately 200 nm (Figs. 2c and 2f). After modification and drug loading, the size increased slightly due to the drug

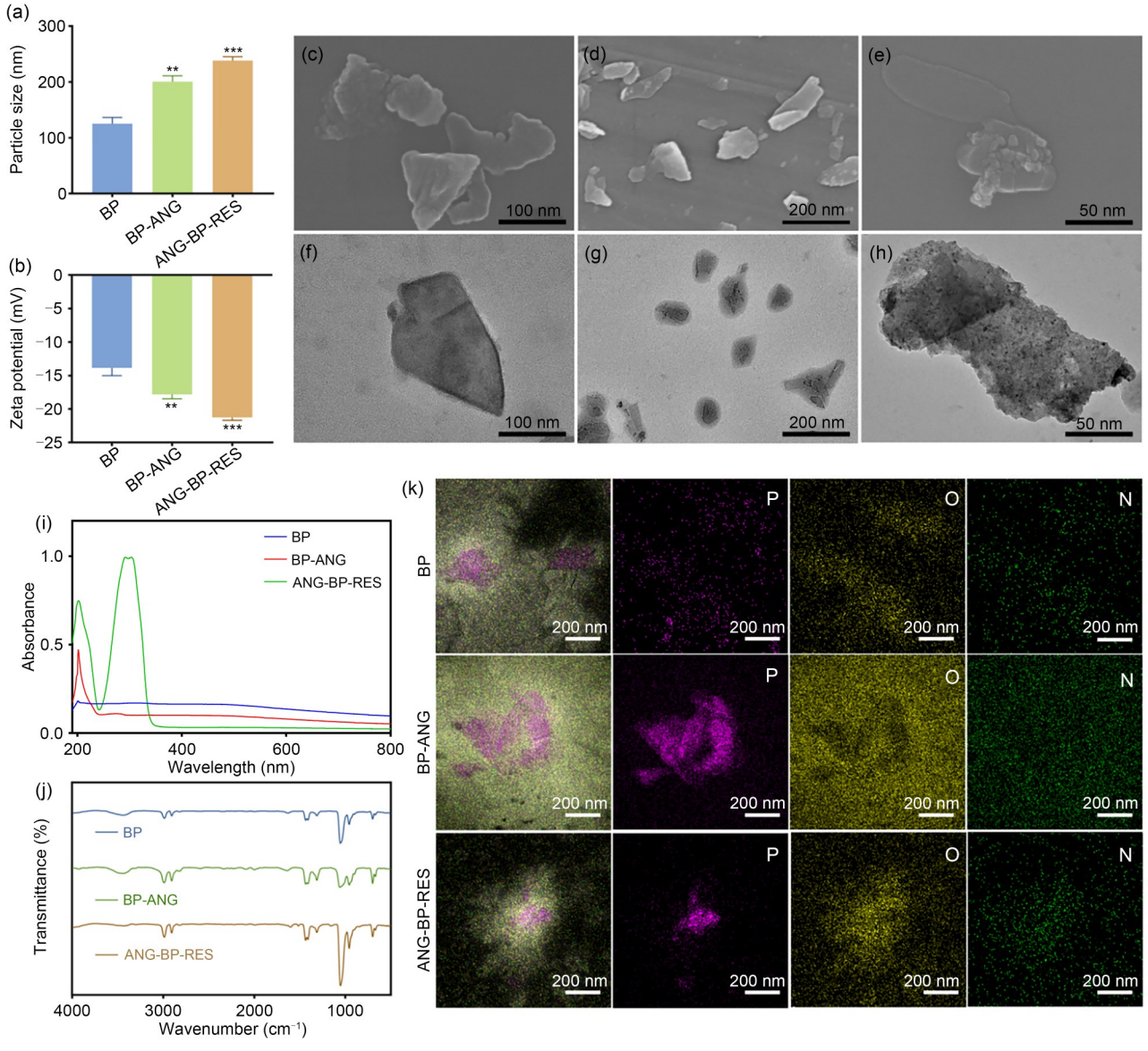

Fig. 2 Characterization of nanosheets. Particle size (a) and potential (b) distributions of BP, BP-ANG, and ANG-BP-RES nanosheets. SEM images of BP (c) and ANG-BP-RES (d, e) nanosheets. TEM diagrams of BP (f) and ANG-BP-RES (g, h). UV full-wavelength scanning images (i) and infrared spectrograms (j) of BP, BP-ANG, and ANG-BP-RES. (k) Scanning transmission electron microscopy (STEM) images of BP, BP-ANG, ANG-BP-RES, and their P, O, and N element mapping. Data are expressed as mean±standard deviation (n=3), $^{**}P$<0.01, $^{***}P$<0.005 vs. BP

loaded between the lamellae of BP nano-tablets. The lamellar structure of the drug remained unchanged before and after modification and drug loading (Figs. 2d, 2e, 2g, and 2h; Fig. S1 in the supplementary information). UV-Vis analysis revealed the characteristic peaks of ANG and RES in ANG-BP-RES at 201.6 and 306 nm, respectively (Fig. 2i). The FTIR results revealed that the characteristic peak of the C=O stretching vibration of ANG-BP-RES improved at 1650 cm^{-1} and the absorption bands at 1538 and 1045 cm^{-1} are assigned to the N–H bending vibration and the C–O stretching vibration, respectively (Fig. 2j). These results confirm that BP was successfully modified by ANG and loaded with RES.

Eventually, scanning transmission electron microscopy (STEM) energy spectrum analysis technology was employed to evaluate the distribution of P, O, and N elements in ANG-BP-RES. The results revealed that the BP surface has no surface coating and contains overlapping P and O elements, hence confirming its preparation (Fig. 2k; Fig. S2a in the supplementary information). After polypeptide modification, P was found to be covered by O in BP-ANG (Fig. 2k; Fig. S2b in the supplementary information), confirming the successful modification of BP by ANG. In ANG-BP-RES (Fig. 2k; Fig. S2c in the supplementary information), the bright region (P) was covered by more dark regions, indicating the increased coverage area of O on P. Further, the area of P in the O region of ANG-BP-RES was larger than that of BP, confirming the successful preparation of the BP-ANG shell–core structure.

3.2 Characterization of the photothermal performance

Further, we evaluated the UV absorption properties of BP, BP-ANG, and ANG-BP-RES. The findings showed that the changes in absorbance (Figs. 3a and 3d; Fig. S3a in the supplementary information) were minimal after modification with peptides and drug loading, but increased over time. This enables easy oxidation of BP since its surface is not coated in chemicals (Fig. 3a). After ANG modification, which slows oxidation and improves the stability of preparation, the shell−core structure was developed. Therefore, the addition of ANG and RES might significantly reduce the decline in absorption value (Fig. 3d), indicating improved stability of ANG-BP-RES compared to BP.

The BP, BP-ANG, and ANG-BP-RES preparations were irradiated with an 808-nm NIR laser for 10 min to evaluate their photothermal performance. The temperatures of these preparations increased throughout the irradiation process, reaching peaks of 40.0, 41.0, and 42.6 °C for BP, BP-ANG, and ANG-BP-RES, respectively, in the first irradiation cycle (Figs. 3b and 3e; Fig. S3b in the supplementary information). The change in peak temperature was recorded after five repetitions of the photoexcitation (PT) cycle (laser on/off). After five PT cycles, we found that the peak temperature of BP, BP-ANG, and ANG-BP-RES decreased from 40.0 to 38.8 °C (Fig. 3b), 41.0 to 40.0 °C (Fig. S3b in the supplementary information), and 42.6 to 42.4 °C (Fig. 3e), respectively. The solutions were scanned at 200–800 nm before and after five cycles of NIR irradiation. Figures 3c and 3f respectively show the UV full-wavelength scanning results of BP and ANG-BP-RES before and after PT irradiation. It can be seen that the results of UV full-wavelength scanning of BP after PT irradiation are quite different, while the overall trend of ANG-BP-RES has not changed. These results confirm that ANG modification significantly enhances the photostability of BP nanosheets by minimizing absorbance degradation. In contrast, the photothermal performance of ANG-modified BP and its stability improved. At 37 °C, both the photothermal stability and absorption of ANG-BP-RES were higher, indicating that its therapeutic benefits might last in the body for long periods.

The highest in vitro drug release from ANG-BP-RES was achieved at pH=5.8, with a release rate of (52.8± 1.24)% within 24 h (Fig. S5 in the supplementary information). In the NIR irradiation group (Fig. 3l), the release rate of ANG-BP-RES was (85.64±3.08)% at pH=5.8 within 24 h. These results confirm that NIR irradiation can stimulate ANG-BP-RES to release RES, and this drug release ability can be further improved at pH=5.8. Additionally, we recorded temperature changes of BP, BP-ANG, and ANG-BP-RES at different powers and concentrations within 10 min. The results showed that BP possessed excellent photothermal properties based on time, concentration, and laser power (Figs. 3g–3i). Similarly, BP-ANG and ANG-BP-RES showed good photothermal performances, which are also dependent on time, concentration, and laser power (Figs. 3j and 3k; Fig. S4 in the supplementary information).

3.3 Evaluation of neuroprotective effect in vitro

After co-culturing SH-SY5Y cells with different concentrations of RES, BP, ANG-BP-RES, and ANG-BP-RES+NIR, the CCK-8 assay was performed to evaluate the cellular activity. The results revealed that, even at a high drug concentration (200 μg/mL), the cellular activity of each group was above 75%, confirming its safety (Fig. 4a).

Then, SH-SY5Y cells were co-cultured with different concentrations of glutamic acid (1.25, 2.5, 5, 10, 20, and 30 mmol/L) to explore the suitable concentration of glutamic acid for modeling. Then, the CCK-8 assay was performed. The findings revealed that in the presence of 20 mmol/L glutamic acid, the cell activity was 33.04%, which was the best modeling concentration (Fig. S6 in the supplementary information). Glutamate-treated SH-SY5Y

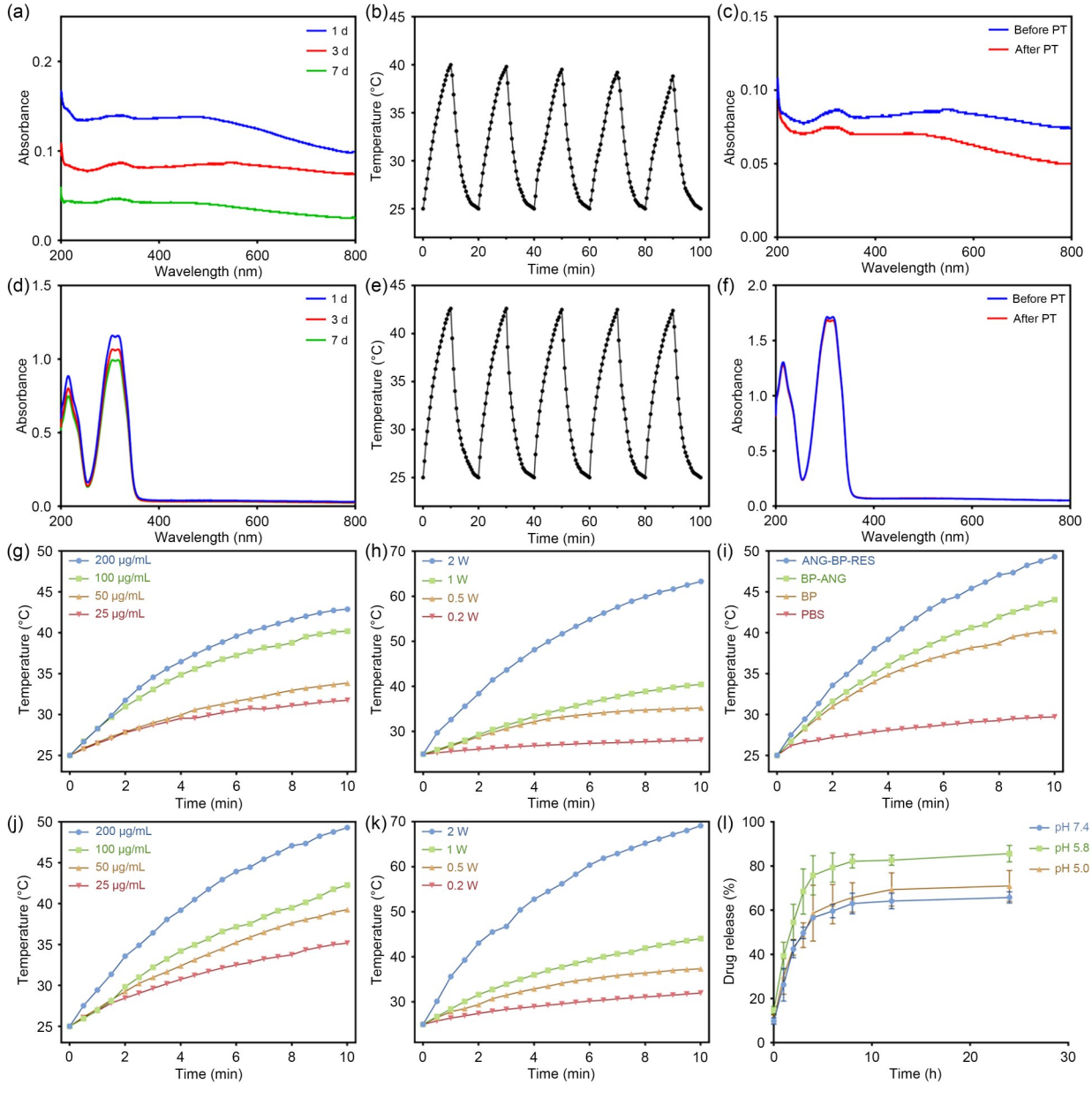

Fig. 3 Photothermal performance evaluation of ANG-BP-RES. The following parameters are shown for BP and ANG-BP-RES: (a, d) their stability in PBS; (b, e) photothermal on/off cycles; (c, f) photothermal stability; and in vitro temperature curves at (g, j) different concentrations, (h, k) different powers, and (i) different groups after irradiation with an 808-nm NIR laser at a power density of 1.0 W/cm^2 for 10 min. (l) In vitro release results of ANG-BP-RES after NIR irradiation. Data are expressed as mean±standard deviation (n=6)

cells were mixed with RES, BP-RES, BP-RES+NIR, ANG-BP-RES, and ANG-BP-RES+NIR at different concentrations (1, 5, 10, 20, 50, and 100 μg/mL). In the ANG-BP-RES+NIR group, cells exhibited extensive apoptosis after modeling (Fig. 4b). However, this apoptotic effect showed dose-dependent attenuation with increasing concentrations of ANG-BP-RES (Fig. 4e). Notably, at higher concentrations (50 and 100 μg/mL), apoptotic cells were scarcely observed. These findings demonstrate that ANG-BP-RES combined with NIR irradiation effectively protects neural cells from apoptosis.

Cerebral vascular disorders pose a significant human health challenge due to their complex pathophysiology that is closely associated with oxygen-free radicals, increased excitatory amino acid release, intracellular calcium excess, and other factors [44]. Studies have shown that free radicals cause ischemic brain damage [45]. After cerebral ischemia, cell membrane permeability increases, which, in addition to decreasing the extravasation and activity of LDH in brain tissues, causes a large influx of calcium ions, resulting in intracellular calcium overload. Besides directly damaging neurons, it can activate enzymatic reactions, promote free

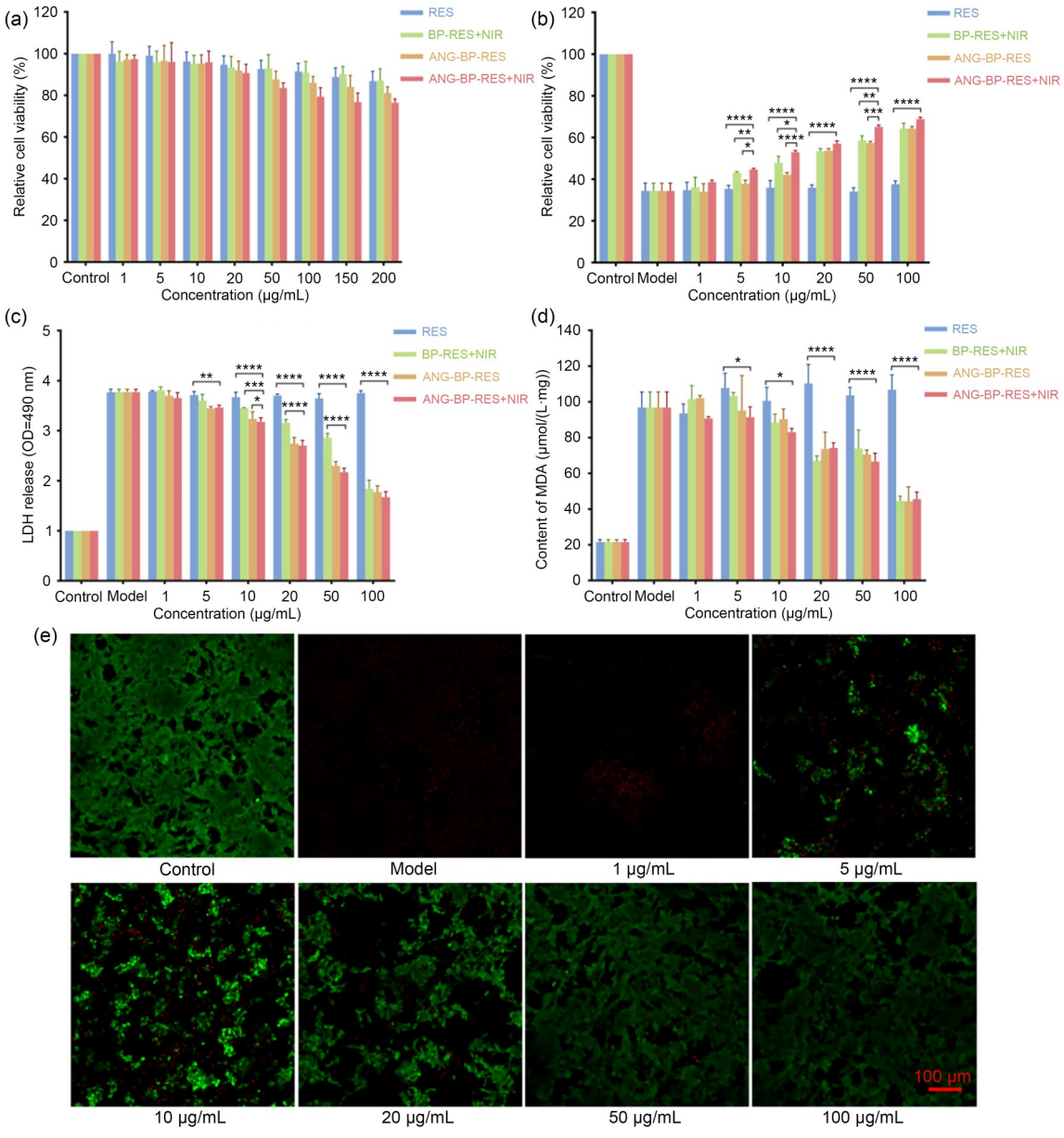

Fig. 4 Evaluation of biocompatibility and neuroprotective effect of ANG-BP-RES in vitro. The effects of different concentrations of RES, BP-RES+NIR, ANG-BP-RES, and ANG-BP-RES+NIR on nerve cell activity before (a) and after (b) modeling and on LDH (c) and MDA (d) release from nerve cells after modeling were evaluated. (e) Live cell staining images at different concentrations of ANG-BP-RES+NIR (scale bar: 100 μm). Data are expressed as mean±standard deviation (n=3), $^{*}P<0.05$, $^{**}P<0.01$, $^{***}P<0.005$, $^{****}P<0.001$

radical production, and damage membrane lipids via peroxidation, hence exacerbating cell damage [45]. Lipid peroxidation comprises a series of free radical reactions on unsaturated fatty acids, which causes brain tissue damage through acute cerebral ischemia [46]. Cui et al. [47] discovered that the free radical levels and MDA content increased in the brains of rats 6 h after cerebral ischemia was induced. This was apparent 12–24 h after the operation before decreasing. The MDA levels immediately increased 2 min after cerebral ischemia, indicating that the free radical levels also increased shortly after ischemia and hypoxia, promoting lipid peroxidation. In summary, the release of LDH and MDA from nerve cells is an important index to evaluate brain tissue damage. Therefore, we assessed the protective effect of ANG-BP-RES on nerve cells by detecting the changes in LDH and MDA release in nerve cells.

The model group included SH-SY5Y cells treated with various concentrations of RES, BP-RES+NIR, ANG-BP-RES, and ANG-BP-RES+NIR (1, 5, 10, 20, 50, and 100 μg/mL). The results revealed that the LDH and MDA release was significantly elevated in the model group, but was suppressed after administration (Figs. 4c and 4d). The

capacity of the ANG-BP-RES+NIR group to suppress LDH and MDA release was substantially higher than that of other groups. Previous studies also indicated that the peptide-modified brain-focused drug delivery system ANG-BP-RES can mitigate the effects of ischemic brain damage by preventing LDH and MDA release from cells.

3.4 In vitro evaluation of BBB permeability

The BBB is important for preventing drugs from entering the brain [48]. However, regulatory chemicals can be transported from the blood across the BBB and BCSFB into the brain. However, due to the inadequate number of channels and significantly reduced surface area, BCSFB has a less significant impact on the material exchange between the brain and blood [49]. Several cell types, including endothelial and peripheral cells, and astrocytes work synergistically to regulate the permeability of the BBB. A combination of a tight connection, an adhesive connection, and the polarity of the top lobe and cavity surface constitute the gating characteristics of BBB [50, 51]. Therefore, most neuroprotective drugs cannot cross the BBB due to their unique properties, making it difficult to treat nervous system diseases.

Herein, a Transwell assay was used to model the BBB to examine the permeability of ANG-BP-RES, a peptide-modified brain-targeted drug delivery system across the BBB. In this system, the bEnd.3 cell line is commonly used to test whether a drug delivery system can cross the BBB in vitro. The experiment was divided into four groups (n=3): (1) Cy5.5, (2) BP-Cy5.5+NIR, (3) ANG-BP-Cy5.5, and (4) ANG-BP-Cy5.5+NIR. Groups (2) and (4) were irradiated with an NIR laser at 1 W/cm^2 (808 nm, 5 min). The results revealed that the permeability of Group (2) was (14.34±1.08)%, which was 1.11 times higher than that of Group (1) after 4 h of culture. The permeability of Group (4) reached (32.47±4.63)%, which was 2.26 times that of Group (3) (Fig. 5e). These findings indicate that this ANG-modified BP nano-tablet drug delivery system can improve the permeability of the BBB, which was further enhanced after NIR laser irradiation.

3.5 In vivo fluorescence imaging

The ability of the designed drug delivery system to induce hemolysis was evaluated before the in vivo investigations. The results revealed that ANG-BP-Cy5.5 induced minor hemolysis (5%), making it suitable for intravenous administration (Fig. S7 in the supplementary information). The difference between BBB permeability and BP nanosheet brain-targeting was examined using the fluorescent labeling method to assess the in vivo brain-targeting capacity of the BP nanosheets. The mice were divided into five groups (n=6): (1) free Cy5.5+NIR, (2) BP-Cy5.5, (3) BP-Cy5.5+NIR, (4) ANG-BP-Cy5.5, and (5) ANG-BP-Cy5.5+NIR. After tail vein administration, all animals were subjected to fluorescence imaging at different time points. No fluorescence was detected in the brains of mice in Group (1) (Fig. 5a; Fig. S8 in the supplementary information).

The fluorescence peaked at 6 h after tail vein injection in the brain tissue. Subsequently, the mice were dissected 6 h after injection to examine the fluorescence intensity of each tissue (Fig. 5b). ANG-modified BP exhibited significantly higher BBB permeability and brain-targeting ability than that of other groups. Statistical analysis of the fluorescence intensity of each tissue revealed that NIR irradiation further improved its brain-targeting (Figs. 5c and 5d). Additionally, the fluorescence intensity levels were lower in the heart and spleen tissues than those in the lung, kidney, and liver tissues. This shows that BP nano-preparation can be readily captured by related organs of the reticuloendothelial system before kidney elimination.

3.6 Pharmacokinetic analysis in vivo

Pharmacokinetic analysis was conducted to evaluate the in vivo performance of ANG-BP-RES. Using the established resveratrol plasma standard curve (Fig. S9 in the supplementary information), we systematically measured resveratrol plasma concentrations at predetermined time intervals following administration across all experimental groups. The plasma concentration−time curve showed that the C_{max} value of the RES group was (5.414±0.951) μg/mL after administration, while that of the ANG-BP-RES+NIR group was 1.85 times that of the RES group, at (10.037±1.027) μg/mL (Fig. 6a; Table S1 in the supplementary information). The $T_{1/2}$ of the ANG-BP-RES+NIR group increased to (2.378±0.123) h, which was 1.09 times that of the RES group. In addition, AUC_{0-t} and MRT_{0-t} of the ANG-BP-RES+NIR group were 2.23 times and 1.14 times those of the RES group, respectively. The changes in the above plasma concentration parameters confirmed that BP nanosheets were successfully modified by the brain-targeted peptide ANG, and the bioavailability of RES was significantly enhanced under NIR irradiation-induced photothermal effects.

Subsequently, based on the resveratrol standard curve for each tissue (Fig. S10 in the supplementary information), we quantified the changes in resveratrol concentration across different tissues at various time points post-administration. Following intravenous injection, the drug concentration–time profile in brain tissue was determined (Fig. 6b), and the corresponding pharmacokinetic parameters were calculated (Table S2 in the supplementary information). The drug concentration reached the peak in the RES group ((0.040±0.003) μg/g) 4 h after administration, while in the

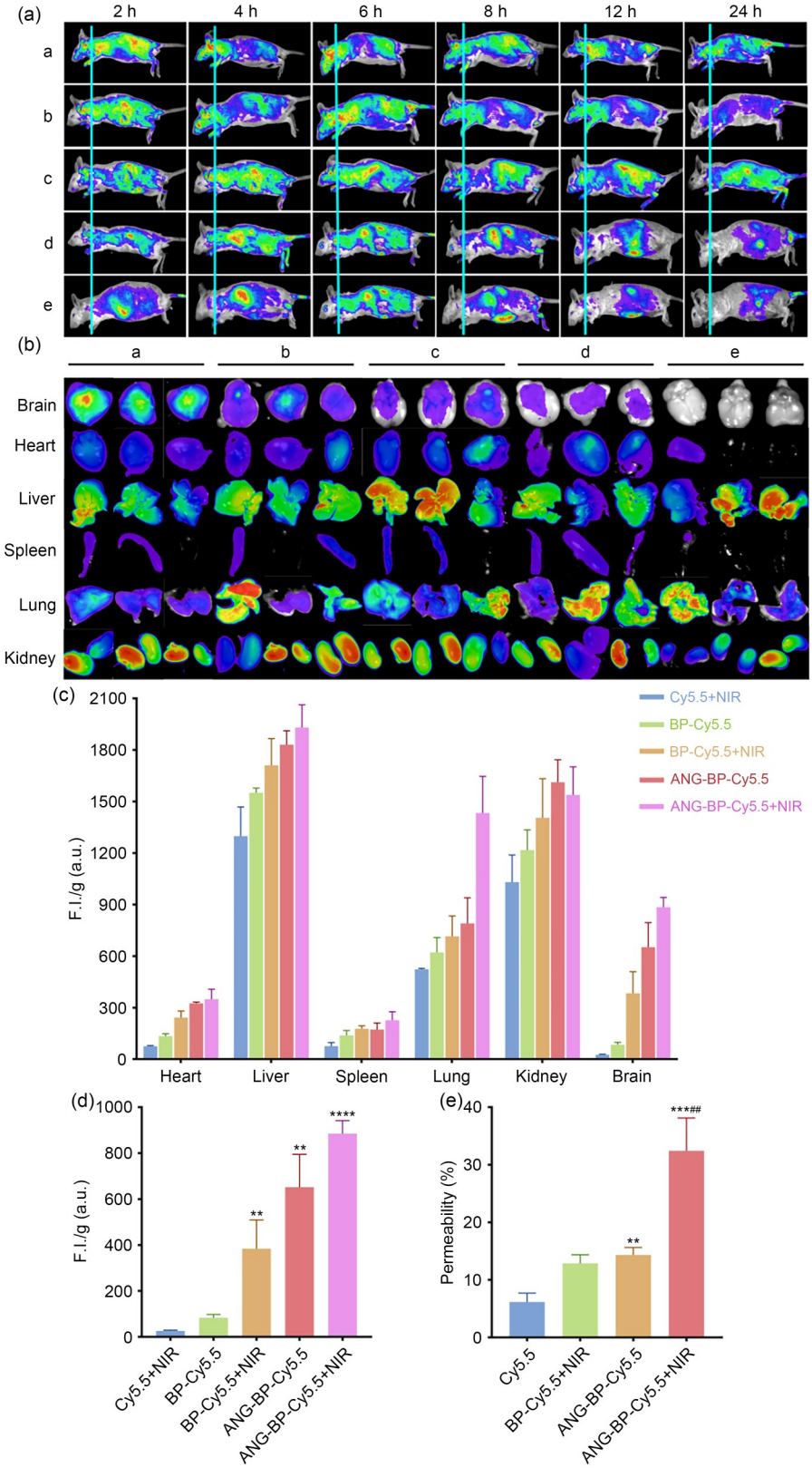

Fig. 5 Evaluation of the in vivo and in vitro BBB permeability of the drug delivery system. (a) Whole body fluorescence imaging of the mice 2–24 h after administration. (b) Fluorescent imaging of main organs in the mice 6 h after administration (a: ANG-BP-Cy5.5+NIR; b: ANG-BP-Cy5.5; c: BP-Cy5.5+NIR; d: BP-Cy5.5; e: Cy5.5+NIR). Fluorescence intensity of main organs (c) and the brain tissue (d) in the mice 6 h after administration ($^{**}P<0.01$, $^{****}P<0.001$ vs. BP-Cy5.5). (e) Evaluation of BBB permeability using a Transwell chamber ($^{**}P<0.01$, $^{***}P<0.005$ vs. BP-Cy5.5+NIR; $^{\#\#}P<0.01$ vs. ANG-BP-Cy5.5). Data are expressed as mean±standard deviation ($n=3$)

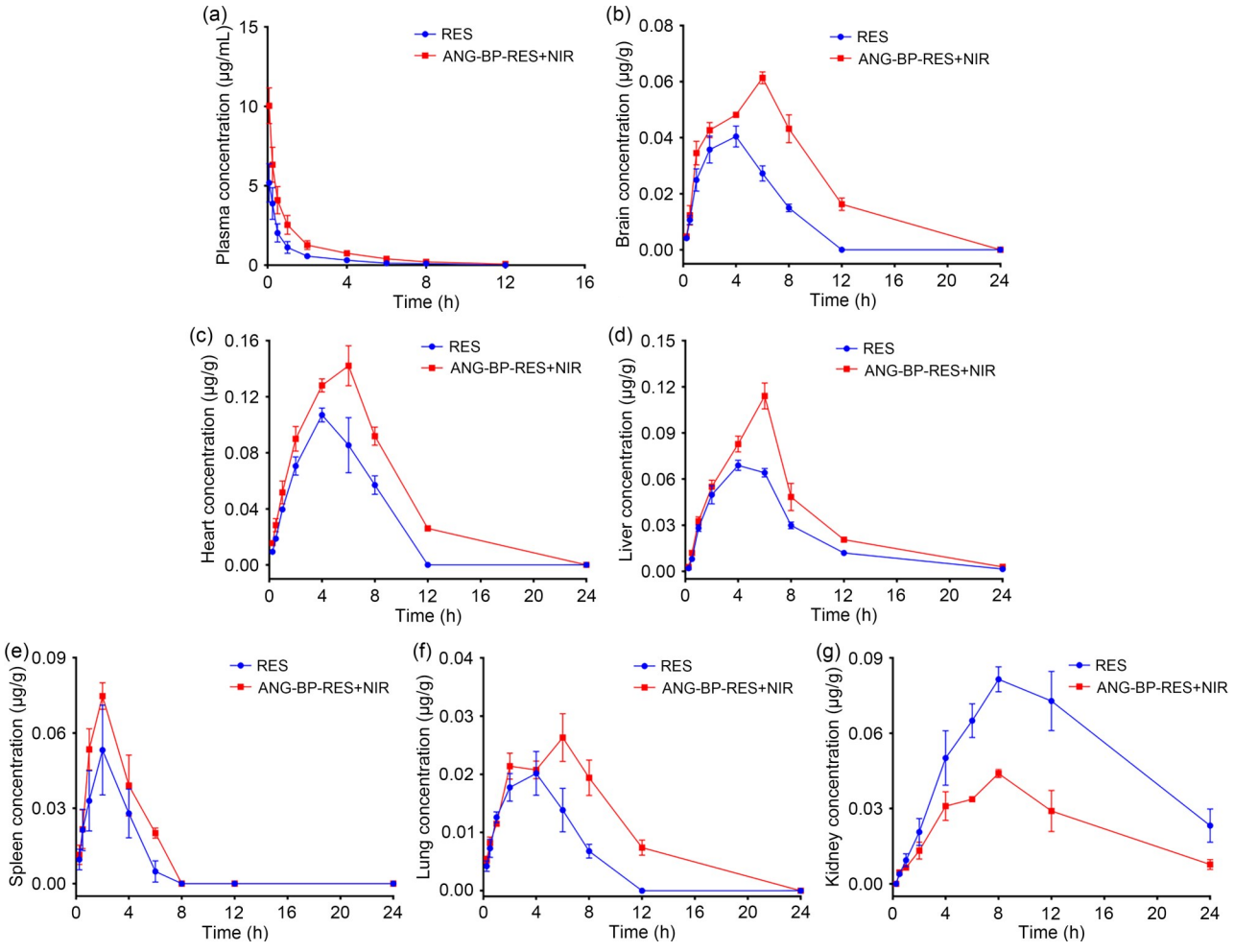

Fig. 6 Concentration–time curves of RES and ANG-BP-RES+NIR in plasma and various tissues. After administration of RES and ANG-BP-RES+NIR, the concentration–time curves from the plasma (a), brain (b), heart (c), liver (d), spleen (e), lungs (f), and kidney (g) were evaluated. Data are expressed as mean±standard deviation (n=6 for (a) and n=3 for the others)

ANG-BP-RES+NIR group, it peaked 6 h after administration ((0.061±0.002) μg/g). The C_{max} of the ANG-BP-RES+NIR group was approximately 1.53 times that of the RES group. Further, the $T_{1/2}$ of the ANG-BP-RES+NIR group increased to (3.114±0.364) h, which was 1.11 times that of the RES group. The AUC_{0-t} and MRT_{0-t} of the ANG-BP-RES+NIR group were 2.10 times and 1.27 times those of the RES group, respectively. These pharmacokinetic changes in the brain tissues confirmed that BP nanosheets were modified by the brain-targeting polypeptide ANG. Under the photothermal effect of NIR irradiation, more ANG-BP-RES might enter the brain through the BBB, further enhancing the therapeutic effect.

Furthermore, the concentration–time curves of other main tissues were detected (Figs. 6c–6g). The concentration in the heart, liver, spleen, and lung of the ANG-BP-RES+NIR group was significantly higher than that of the RES group, while the concentration in the kidney was lower than that of the RES group. After BP nanosheets were modified by the brain-targeting polypeptide ANG and loaded with drugs, the drug distribution changed in the body due to the brain-targeting ability and nano-size of the preparation. The concentration in the kidney tissues in the RES group was higher than that in the ANG-BP-RES+NIR group, which may be because BP nano-preparation was easily captured by related organs in the reticuloendothelial system before renal elimination, resulting in a decrease in its content in the kidney tissues.

3.7 Evaluation of anti-ischemic brain injury in vivo

To assess the anti-ischemic stroke effect, the behavior, brain water content, and cerebral infarct area of rats in each group were compared 24 h after drug administration. The behavioral score showed that compared with the blank group, the behavior of the model group indicated clear neurological abnormalities 24 h after the operation (Fig. 7a).

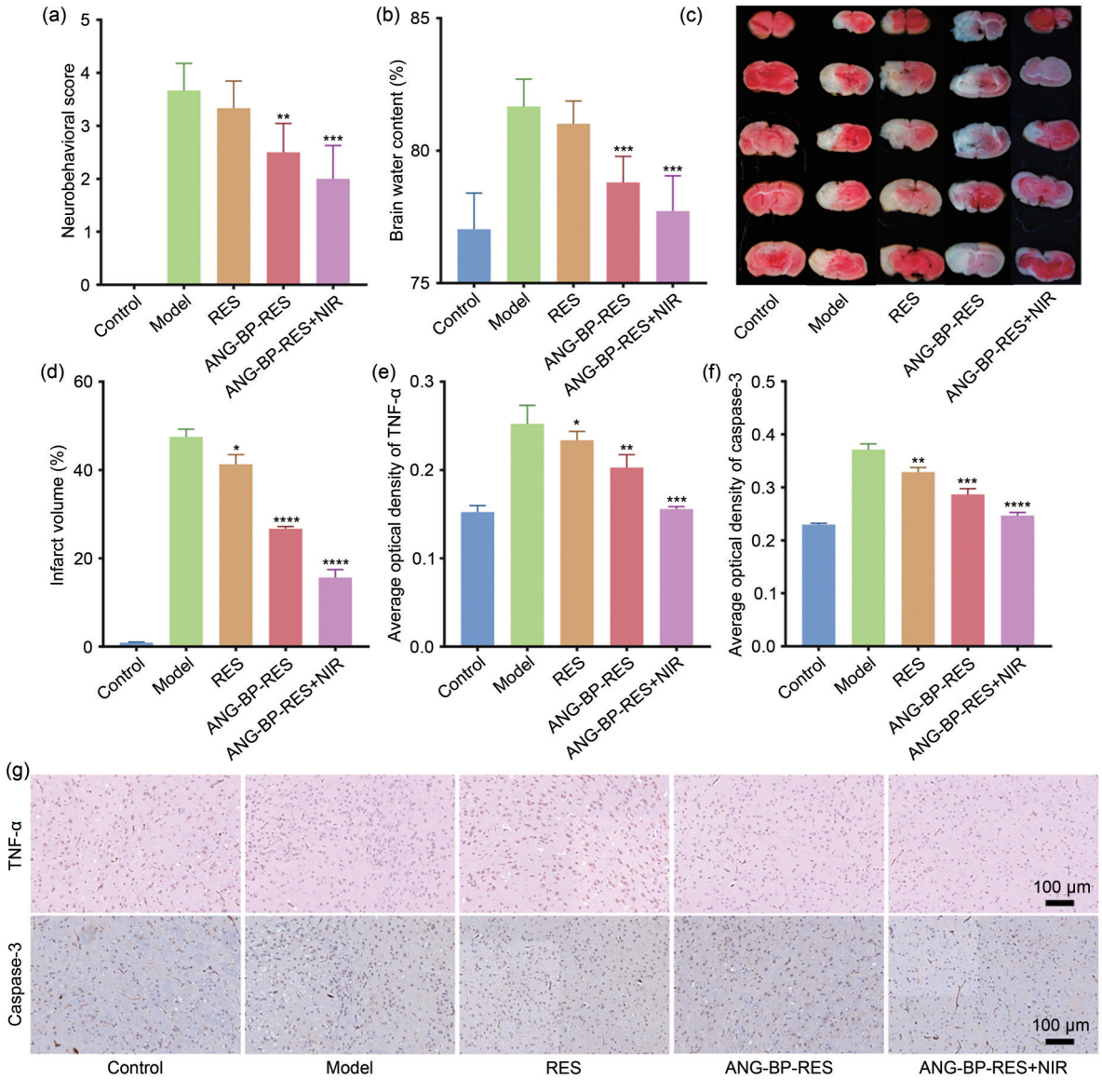

Fig. 7 Evaluation of anti-ischemic brain injury in vivo. The behavioral score (a), brain water content (b), TTC staining results (c), and area of cerebral infarction (d) were assessed. The average optical densities of TNF-α (e) and caspase-3 (f). Data are expressed as mean±standard deviation (n=6 for (d) and n=3 for (a, b, e, f)), $^{*}P$<0.05, $^{**}P$<0.01, $^{***}P$<0.005, $^{****}P$<0.001 vs. the model group. (g) Immunohistochemical staining results of brain tissue slices from the control, model, RES administration, ANG-BP-RES, and ANG-BP-RES+NIR groups (scale bar: 100 μm)

Although the mice in the RES and ANG-BP-RES groups still exhibited symptoms of neurobehavioral disorders, these symptoms improved in the RES group compared with the model group. Further, these symptoms were significantly alleviated in the ANG-BP-RES+NIR group. The brain water content in the blank group was (77.03±1.25)%, while that in the ischemic brain tissues of the model group was (81.67±0.94)%, showing a significant increase 24 h after the operation (Fig. 7b). Compared with the model group, the brain water content of the mice in each group was significantly reduced, and was (77.72±1.22)% in the ANG-BP-RES+NIR group, indicating a significantly higher therapeutic effect than that of the other drug groups. The results of the cerebral infarct area showed that after 24 h of MCAO reperfusion in mice, the ischemic brain tissue of the model group had obvious infarction, and the infarct area was approximately (47.50±1.43)% (Figs. 7c and 7d). Compared with the model group, the infarct area of mice in each group was reduced after modeling and administration. The infarct area of the ANG-BP-RES+NIR group was (15.67±1.58)%, which was significantly smaller than that of other administration groups.

The cytokine TNF-α has several biological functions [52]. It can activate neutrophils to kill pathogenic microorganisms, stimulate monocytes and other cells to produce other cytokines, such as interleukin (IL)-1 and IL-6, and activate

B lymphocytes to produce antibodies, which significantly improves immune suppression, enhancing and protecting autoimmune function [53]. The TNF-α levels are low in normal brain tissues to maintain the growth, differentiation, development, and function of nervous tissues [54]. During ischemic brain injury, the TNF-α produced by astrocytes, microglia, and nerve cells can enhance the permeability of endothelial cells and increase the adhesion function of neutrophils, monocytes, and lymphocytes to the surface of vascular endothelial cells, thus changing the permeability of the BBB and promoting inflammatory cells to enter the nervous tissues [55, 56]. Particularly, TNF-α can enhance its expression and adhesion to inflammatory cells by increasing the effect of tissue factors and platelet-activating factors on adhesion receptor molecules [57]. Caspase-3, belonging to the IL-1β converting enzyme (ICE) family, is a protease involved in cellular apoptosis [58]. Recently, caspase-3 was found to be involved in the pathological process of neuronal injury after cerebral ischemia, establishing its role in cerebral ischemia [59]. Accumulating evidence has shown that caspase-3 is also involved in several biological processes other than apoptosis [60]. A previous study found that the expression of caspase-3 in neonatal neural precursor cells in the subventricular zone of the hippocampus and dentate gyrus increased significantly during recovery from stroke [61]. Although caspase-3 is widely co-located with newly generated neural stem cells, it shows no signs of apoptosis. Neural precursor cells were extracted from the subventricular zone and dentate gyrus of the hippocampus in ischemic mice and cultured in vitro. The results showed that caspase-3 limited the self-renewal ability of neural precursor cells but it did not participate in apoptosis. Subsequent investigations revealed that inhibiting the activity of caspase-3 can enhance the proliferation and migration of neural precursor cells in the subventricular zone via suppression of Akt phosphorylation. This, in turn, leads to increased conversion of newborn neural stem cells into neurons and restoration of neurological function following a stroke. These findings indicate that caspase-3 is the key molecule that limits the regeneration of nerves in the brain after a stroke. Overall, this study sought to investigate the changes in TNF-α and caspase-3 to evaluate the therapeutic effect of ANG-BP-RES on ischemic brain injury in vivo.

After 24 h of administration, the mice were perfused and dissected. The changes in caspase-3 and TNF-α in the brain tissues of each group were detected using immunohistochemistry. The results showed that the average optical density of TNF-α and caspase-3 in the blank group was 0.152± 0.006 and 0.230±0.002, respectively, while these values increased to 0.252±0.017 and 0.371±0.009, respectively, after modeling (Figs. 7e–7g; Table S3 in the supplementary information). After administration, the expression of caspase-3 and TNF-α was significantly inhibited. In the ANG-BP-RES+NIR group, the inhibition of caspase-3 and TNF-α expression was significantly higher than that of other groups. In this group, the average optical density of TNF-α and caspase-3 decreased to 0.156±0.002 and 0.247± 0.005, respectively. These results established that the peptide-modified brain-targeted BP nano-tablet delivery system can inhibit caspase-3 and TNF-α expression, exerting an anti-ischemic brain damage effect.

3.8 H&E staining

A nano-drug delivery system, whose diameter ranges between 1 and 1000 nm, can help deliver targeted drugs to different organisms [62]. Approximately 12 000 articles have been published in the last decade about nano-drug delivery systems. These studies showed that evaluating the biological safety of these systems is crucial before their clinical application [63]. The aforementioned experiments confirmed that this peptide-modified brain-targeted drug delivery system (ANG-BP-RES) has low cytotoxicity and a slight hemolytic effect. Therefore, we evaluated the short-term tissue toxicity of ANG-BP-RES using H&E staining to verify whether it is worthy of further exploration.

To investigate the tissue toxicity of each component at the highest dosage, the biological safety of RES, ANG-BP-RES, and ANG-BP-RES+NIR after continuous injection of the maximum dosage for one week was investigated. The results showed that although the maximum dose of PBS, RES, ANG-BP-RES, and ANG-BP-RES+NIR was injected daily for one week, there was no obvious inflammatory reaction in the main tissues of mice (Fig. 8). Additionally, the mice in each group did not exhibit any weight loss within one week after continuous administration (Fig. S11 in the supplementary information). These results suggest that the drugs in each group have no obvious tissue toxicity.

4 Conclusions

In summary, ANG-BP-RES, a peptide-modified BP nanoparticle-based brain-targeted drug delivery system was developed, which can effectively deliver drugs into the brain through the BBB. It has the advantages of small volume, high stability, good photothermal effect, and brain-targeting capability. In vitro and in vivo experiments demonstrated that ANG-BP-RES can inhibit the release of LDH and MDA in nerve cells. It can also suppress caspase-3 and TNF-α expression in brain tissues to ameliorate ischemic brain damage, significantly improving the behavioral disorder caused by cerebral ischemia in mice, and reducing the degree of brain edema and cerebral infarction. Furthermore, due to its high biocompatibility, it is a promising option for future clinical applications. Considering the more extensive

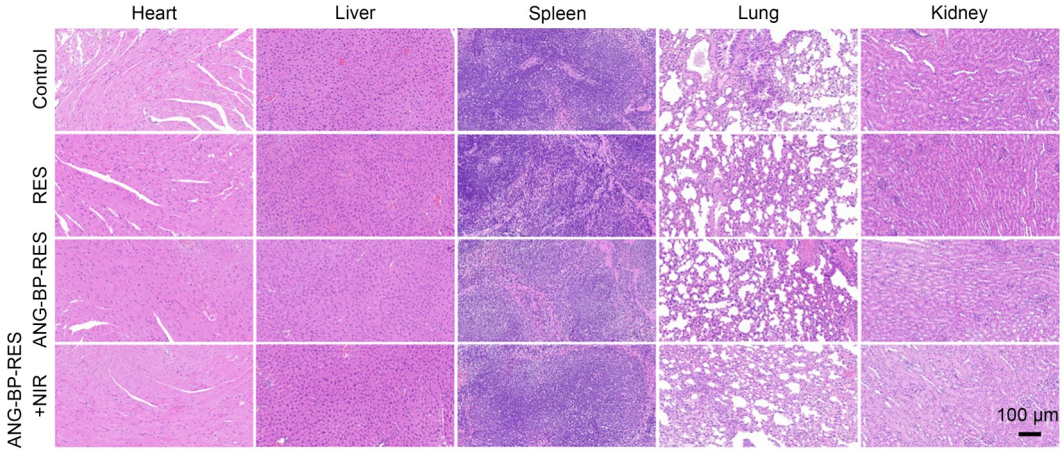

Fig. 8 H&E staining results showing the effect of RES, ANG-BP-RES, and ANG-BP-RES+NIR on various tissues one week after continuous administration (scale bar: 100 μm)

application of laser technology in various medical fields, we believe that this new approach of controlled and brain-targeted release of drugs using BP nanosheets is ideal for treating and preventing ischemic stroke. This preparation can also be used as a general carrier for loading drugs to treat other diseases, making it a new strategy for treating other brain diseases.

Supplementary Information The online version contains supplementary material available at https://doi.org/10.1631/bdm.2400176.

Acknowledgements This work is funded by the National Natural Science Foundation of China (No. 81960334), the Guiding Plan of Xinjiang Production Construction Corps (No. 2022ZD007), the Science and Technology Innovation Leading Talents Program of Guangdong Province (No. 2019TX05C343), the Basic and Applied Basic Research Foundation of Guangdong Province-Regional Joint Fund-Key Projects (No. 2019B1515120043), and the Project supported by the State Key Laboratory of Luminescence and Applications (No. SKLA-2020-03). The authors also acknowledge the support from Instrumental Analysis Center of Shenzhen University (Xili Campus) and Instrumental Analysis Center of Shihezi University.

Author contributions XT, HZ, WC, and MLZ are responsible for proposing research topics and experimental ideas and designing research schemes. MLZ, TJF, SJY, JL, and JH are responsible for the experimental research process. TJF, SJY, JL, JH, BH, and KZ are responsible for material support and data collection. MLZ is responsible for drafting and revising the paper. XT, WC, and HZ are responsible for technical guidance and revision of the final version of the manuscript.

Declarations

Conflict of interest The authors declare that they have no conflict of interest.

Ethical approval The guidelines for animal protection adopted in experiments were formulated by the Animal Protection Committee of the First Affiliated Hospital of Shihezi University. Animal welfare and experimental process were carried out according to the regulations of the Animal Ethics Committee of the First Affiliated Hospital of Shihezi University (Approval No. A2022-100-01).

Data availability The data that support the findings of this study are available from the corresponding authors upon reasonable request.

References

1. Sasane R, Bartels A, Field M et al (2021) Parkinson disease among patients treated for benign prostatic hyperplasia with α1 adrenergic receptor antagonists. J Clin Invest 131(11):e145112. https://doi.org/10.1172/JCI145112
2. Paul S, Candelario-Jalil E (2021) Emerging neuroprotective strategies for the treatment of ischemic stroke: an overview of clinical and preclinical studies. Exp Neurol 335:113518. https://doi.org/10.1016/j.expneurol.2020.113518
3. Herpich F, Rincon F (2020) Management of acute ischemic stroke. Crit Care Med 48(11):1654–1663. https://doi.org/10.1097/ccm.0000000000004597
4. Hopfner F, Müller SH, Steppat D et al (2019) No association between Parkinson disease and autoantibodies against NMDA-type glutamate receptors. Transl Neurodegener 8:11. https://doi.org/10.1186/s40035-019-0153-0
5. Morofuji Y, Nakagawa S (2020) Drug development for central nervous system diseases using in vitro blood-brain barrier models and drug repositioning. Curr Pharm Des 26(13):1466–1485. https://doi.org/10.2174/1381612826666200224112534
6. Tang SN, He ZL, Liang GW et al (2018) Pulse duration dependent nonlinear optical response in black phosphorus dispersions. Opt Commun 406:244–248. https://doi.org/10.1016/j.optcom.2016.11.036
7. Nogueira RG, Jadhav AP, Haussen DC et al (2018) Thrombectomy 6 to 24 hours after stroke with a mismatch between deficit and infarct. N Engl J Med 378(1):11–21. https://doi.org/10.1056/nejmoa1706442
8. Albers GW, Marks MP, Kemp S et al (2018) Thrombectomy for stroke at 6 to 16 hours with selection by perfusion imaging. N Engl J Med 378(8):708–718. https://doi.org/10.1056/nejmoa1713973
9. Ajoolabady A, Wang SY, Kroemer G et al (2021) Targeting autophagy in ischemic stroke: from molecular mechanisms to clinical therapeutics. Pharmacol Ther 225:107848. https://doi.org/10.1016/j.pharmthera.2021.107848
10. Umlauf BJ, Shusta EV (2019) Exploiting BBB disruption for the delivery of nanocarriers to the diseased CNS. Curr Opin Biotechnol 60:146–152.

https://doi.org/10.1016/j.copbio.2019.01.013
11. Li XM, Tsibouklis J, Weng TT et al (2017) Nano carriers for drug transport across the blood-brain barrier. J Drug Target 25(1):17–28. https://doi.org/10.1080/1061186X.2016.1184272
12. Mdzinarishvili A, Sutariya V, Talasila PK et al (2013) Engineering triiodothyronine (T3) nanoparticle for use in ischemic brain stroke. Drug Deliv Transl Res 3(4):309–317. https://doi.org/10.1007/s13346-012-0117-8
13. Emerich DF, Silva E, Ali O et al (2010) Injectable VEGF hydrogels produce near complete neurological and anatomical protection following cerebral ischemia in rats. Cell Transplant 19(9): 1063–1071. https://doi.org/10.3727/096368910X498278
14. Nair SB, Dileep A, Rajanikant GK (2012) Nanotechnology based diagnostic and therapeutic strategies for neuroscience with special emphasis on ischemic stroke. Curr Med Chem 19(5):744–756. https://doi.org/10.2174/092986712798992138
15. Rampino A, Borgogna M, Blasi P et al (2013) Chitosan nanoparticles: preparation, size evolution and stability. Int J Pharm 455(1–2):219–228. https://doi.org/10.1016/j.ijpharm.2013.07.034
16. Soares PIP, Sousa AI, Silva JC et al (2016) Chitosan-based nanoparticles as drug delivery systems for doxorubicin: optimization and modelling. Carbohydr Polym 147:304–312. https://doi.org/10.1016/j.carbpol.2016.03.028
17. Gao WW, Zhang Y, Zhang QZ et al (2016) Nanoparticle-hydrogel: a hybrid biomaterial system for localized drug delivery. Ann Biomed Eng 44(6):2049–2061. https://doi.org/10.1007/s10439-016-1583-9
18. Tao W, Zhu XB, Yu XH et al (2017) Black phosphorus nanosheets as a robust delivery platform for cancer theranostics. Adv Mater 29(1):1603276. https://doi.org/10.1002/adma.201603276
19. Chen WS, Huang QY, Ou WZ et al (2014) Self-reporting liposomes for intracellular drug release. Small 10(7):1261–1265. https://doi.org/10.1002/smll.201302698
20. Sun ZB, Xie HH, Tang SY et al (2015) Ultrasmall black phosphorus quantum dots: synthesis and use as photothermal agents. Angew Chem Int Ed 54(39):11526–11530. https://doi.org/10.1002/anie.201506154
21. Li HX, Zhao KC, Jiang JJ et al (2023) Research progress on black phosphorus hybrids hydrogel platforms for biomedical applications. J Biol Eng 17(1):8. https://doi.org/10.1186/s13036-023-00328-w
22. Shao JD, Xie HH, Huang H et al (2016) Biodegradable black phosphorus-based nanospheres for in vivo photothermal cancer therapy. Nat Commun 7:12967. https://doi.org/10.1038/ncomms12967
23. Arora D, Jaglan S (2018) Therapeutic applications of resveratrol nanoformulations. Environ Chem Lett 16(1):35–41. https://doi.org/10.1007/s10311-017-0660-0
24. Diaz-Gerevini GT, Repossi G, Dain A et al (2016) Beneficial action of resveratrol: how and why? Nutrition 32(2):174–178. https://doi.org/10.1016/j.nut.2015.08.017
25. Singh AP, Singh R, Verma SS et al (2019) Health benefits of resveratrol: evidence from clinical studies. Med Res Rev 39(5): 1851–1891. https://doi.org/10.1002/med.21565
26. Raj P, Louis XL, Thandapilly SJ et al (2014) Potential of resveratrol in the treatment of heart failure. Life Sci 95(2):63–71. https://doi.org/10.1016/j.lfs.2013.12.011
27. Elshaer M, Chen YR, Wang XJ et al (2018) Resveratrol: an overview of its anti-cancer mechanisms. Life Sci 207:340–349. https://doi.org/10.1016/j.lfs.2018.06.028
28. Rauf A, Imran M, Suleria HAR et al (2017) A comprehensive review of the health perspectives of resveratrol. Food Funct 8(12):4284–4305. https://doi.org/10.1039/C7FO01300K
29. Huang J, Huang NQ, Xu SF et al (2021) Signaling mechanisms underlying inhibition of neuroinflammation by resveratrol in neurodegenerative diseases. J Nutr Biochem 88:108552. https://doi.org/10.1016/j.jnutbio.2020.108552
30. Ding ZF, Cao JW, Shen Y et al (2018) Resveratrol promotes nerve regeneration via activation of p300 acetyltransferase-mediated VEGF signaling in a rat model of sciatic nerve crush injury. Front Neurosci 12:341. https://doi.org/10.3389/fnins.2018.00341
31. Zhang SO, Botchway BOA, Zhang Y et al (2019) Resveratrol can inhibit Notch signaling pathway to improve spinal cord injury. Ann Anat 223:100–107. https://doi.org/10.1016/j.aanat.2019.01.015
32. Amri A, Chaumeil JC, Sfar S et al (2012) Administration of resveratrol: what formulation solutions to bioavailability limitations? J Contr Release 158(2):182–193. https://doi.org/10.1016/j.jconrel.2011.09.083
33. Davidov-Pardo G, McClements DJ (2015) Nutraceutical delivery systems: resveratrol encapsulation in grape seed oil nanoemulsions formed by spontaneous emulsification. Food Chem 167:205–212. https://doi.org/10.1016/j.foodchem.2014.06.082
34. Rius C, Abu-Taha M, Hermenegildo C et al (2010) *Trans*- but not *Cis*-resveratrol impairs angiotensin-II–mediated vascular inflammation through inhibition of NF-κB activation and peroxisome proliferator-activated receptor-γ upregulation. J Immunol 185(6):3718–3727. https://doi.org/10.4049/jimmunol.1001043
35. Planas JM, Alfaras I, Colom H et al (2012) The bioavailability and distribution of *trans*-resveratrol are constrained by ABC transporters. Arch Biochem Biophys 527(2):67–73. https://doi.org/10.1016/j.abb.2012.06.004
36. Radko Y, Christensen KB, Christensen LP (2013) Semi-preparative isolation of dihydroresveratrol-3-O-β-D-glucuronide and four resveratrol conjugates from human urine after oral intake of a resveratrol-containing dietary supplement. J Chromatogr B Analyt Technol Biomed Life Sci 930:54–61. https://doi.org/10.1016/j.jchromb.2013.05.002
37. Demeule M, Régina A, Ché C et al (2008) Identification and design of peptides as a new drug delivery system for the brain. J Pharmacol Exp Ther 324(3):1064–1072. https://doi.org/10.1124/jpet.107.131318
38. Demeule M, Currie JC, Bertrand Y et al (2008) Involvement of the low-density lipoprotein receptor-related protein in the transcytosis of the brain delivery vector Angiopep-2. J Neurochem 106(4):1534–1544. https://doi.org/10.1111/j.1471-4159.2008.05492.x
39. Zhu JJ, Zhang Y, Chen XJ et al (2021) Angiopep-2 modified lipid-coated mesoporous silica nanoparticles for glioma targeting therapy overcoming BBB. Biochem Biophys Res Commun 534:902–907. https://doi.org/10.1016/j.bbrc.2020.10.076
40. An S, He DS, Wagner E et al (2015) Peptide-like polymers exerting effective glioma-targeted siRNA delivery and release for therapeutic application. Small 11(38):5142–5150. https://doi.org/10.1002/smll.201501167
41. Régina A, Demeule M, Ché C et al (2008) Antitumour activity of ANG1005, a conjugate between paclitaxel and the new brain delivery vector Angiopep-2. Br J Pharmacol 155(2):185–197. https://doi.org/10.1038/bjp.2008.260

42. Drappatz J, Brenner A, Wong ET et al (2013) Phase I study of GRN1005 in recurrent malignant glioma. Clin Cancer Res 19(6):1567–1576. https://doi.org/10.1158/1078-0432.CCR-12-2481
43. Longa EZ, Weinstein PR, Carlson S et al (1989) Reversible middle cerebral artery occlusion without craniectomy in rats. Stroke 20(1):84–91. https://doi.org/10.1161/01.str.20.1.84
44. Hu R, Yin CL, Wu N et al (2009) Traditional Chinese herb *Dihuang Yinzi* (*DY*) plays neuroprotective and anti-dementia role in rats of ischemic brain injury. J Ethnopharmacol 121(3): 444–450. https://doi.org/10.1016/j.jep.2008.09.035
45. Huang YT, Li S, Wang YD et al (2023) A novel 5-chloro-*N*-phenyl-1H-indole-2-carboxamide derivative as brain-type glycogen phosphorylase inhibitor: validation of target PYGB. Molecules 28(4):1697. https://doi.org/10.3390/molecules28041697
46. Anthonymuthu TS, Kenny EM, Bayır H (2016) Therapies targeting lipid peroxidation in traumatic brain injury. Brain Res 1640(Pt A):57–76. https://doi.org/10.1016/j.brainres.2016.02.006
47. Cui XL, Song HQ, Su J (2017) Curcumin attenuates hypoxic-ischemic brain injury in neonatal rats through induction of nuclear factor erythroid-2-related factor 2 and heme oxygenase-1. Exp Ther Med 14(2):1512–1518. https://doi.org/10.3892/etm.2017.4683
48. Upadhyay RK (2014) Drug delivery systems, CNS protection, and the blood brain barrier. BioMed Res Int 2014:869269. https://doi.org/10.1155/2014/869269
49. Abbott NJ (2005) Dynamics of CNS barriers: evolution, differentiation, and modulation. Cell Mol Neurobiol 25(1):5–23. https://doi.org/10.1007/s10571-004-1374-y
50. Jain KK (2012) Nanobiotechnology-based strategies for crossing the blood-brain barrier. Nanomedicine 7(8):1225–1233. https://doi.org/10.2217/nnm.12.86
51. Furtado D, Björnmalm M, Ayton S et al (2018) Overcoming the blood–brain barrier: the role of nanomaterials in treating neurological diseases. Adv Mater 30(46):1801362. https://doi.org/10.1002/adma.201801362
52. McGeehan GM, Uhl J (1996) TNF-α in human diseases. Curr Pharm Des 2(6):662–667. https://doi.org/10.2174/1381612802666221004191458
53. Gough NR (2016) Impairing cognition with TNF-α. Sci Signal 9(409):ec1. https://doi.org/10.1126/scisignal.aaf1771
54. Liu F, Sun XL, Zhang YX et al (2018) Curative effects of GM1 in the treatment of severe ischemic brain injury and its effects on serum TNF-α and NDS. Exp Ther Med 15(6):4851–4855. https://doi.org/10.3892/etm.2018.5995
55. Amin N, Chen SJ, Ren QN et al (2021) Hypoxia inducible factor-1α attenuates ischemic brain damage by modulating inflammatory response and glial activity. Cells 10(6):1359. https://doi.org/10.3390/cells10061359
56. Xu M, Zhou GM, Wang LH et al (2016) Inhibiting high-mobility group box 1 (HMGB1) attenuates inflammatory cytokine expression and neurological deficit in ischemic brain injury following cardiac arrest in rats. Inflammation 39(4):1594–1602. https://doi.org/10.1007/s10753-016-0395-2
57. Lin CP, Tang X, Shi ZY et al (2018) Serum tumor necrosis factor α levels are associated with new ischemic brain lesions after carotid artery stenting. J Vasc Surg 68(3):771–778. https://doi.org/10.1016/j.jvs.2017.11.085
58. Asadi M, Taghizadeh S, Kaviani E et al (2022) Caspase-3: structure, function, and biotechnological aspects. Biotechnol Appl Biochem 69(4):1633–1645. https://doi.org/10.1002/bab.2233
59. Zhao H, Xu M, Chu GL (2017) Association between myocardial cell apoptosis and calpain-1/caspase-3 expression in rats with hypoxic-ischemic brain damage. Mol Med Rep 15(5):2727–2731. https://doi.org/10.3892/mmr.2017.6341
60. Li ZX, Xiao GX, Wang HY et al (2021) A preparation of *Ginkgo biloba* L. leaves extract inhibits the apoptosis of hippocampal neurons in post-stroke mice via regulating the expression of Bax/Bcl-2 and Caspase-3. J Ethnopharmacol 280:114481. https://doi.org/10.1016/j.jep.2021.114481
61. Hu C, Huang YY, Wu LZ et al (2021) Apoptosis and necroptosis occur in the different brain regions of hippocampus in a rat model of hypoxia asphyxia. Int J Neurosci 131(9):843–853. https://doi.org/10.1080/00207454.2020.1759586
62. Aminu N, Bello I, Umar NM et al (2020) The influence of nanoparticulate drug delivery systems in drug therapy. J Drug Deliv Sci Technol 60:101961. https://doi.org/10.1016/j.jddst.2020.101961
63. Khizar S, Alrushaid N, Alam Khan F et al (2023) Nanocarriers based novel and effective drug delivery system. Int J Pharm 632: 122570. https://doi.org/10.1016/j.ijpharm.2022.122570